# The SU(3) twisted gradient flow strong coupling without topology freezing

**Claudio Bonanno,**[a] **Jorge Luis Dasilva Golán,**[b] **Massimo D'Elia,**[c] **Margarita García Pérez,**[a] **Andrea Giorgieri**[c]

[a] *Instituto de Física Téorica UAM-CSIC, Calle Nicolás Cabrera 13-15, Universidad Autónoma de Madrid, Cantoblanco, E-28049 Madrid, Spain*

[b] *Physics Deparment, Brookhaven National Laboratory, Upton, New York 11973, USA*

[c] *Dipartimento di Fisica dell'Università di Pisa & INFN Sezione di Pisa, Largo Pontecorvo 3, I-56127 Pisa, Italy*

*E-mail:* claudio.bonanno@csic.es, jgolandas@bnl.gov, massimo.delia@unipi.it, margarita.garcia@csic.es, andrea.giorgieri@phd.unipi.it

Abstract: We investigate the role of topology in the lattice determination of the renormalized strong coupling via the gradient flow. This is done adopting the Parallel Tempering on Boundary Conditions to deal with the infamous topological freezing problem that affects standard local updating algorithms. We show that, even in the presence of severe topological freezing, both algorithms yield the same strong coupling once projected onto a fixed topological sector. Moreover, we show that using a non-projected definition of the coupling leads to the same step-scaling sequence. This means that projecting the coupling onto a fixed topological sector does not affect the determination of the dynamically-generated scale of the theory $\Lambda$.

Keywords: Vacuum Structure and Confinement, Algorithms and Theoretical Developments, Lattice Quantum Field Theory

## Contents



## 1 Introduction

The limitations of the Standard Model of Particle Physics in providing satisfactory explanations for various experimental observations are widely acknowledged. These include neutrino masses, Dark Matter and strong-CP conservation, among others. As a result, significant theoretical and experimental efforts have been focused on the search for Physics beyond the Standard Model in recent decades. Research in this field has led to the need for more precise and refined theoretical predictions of experimentally-measurable quantities within the framework of the Standard Model itself.

In this respect, it has been emphasized that reducing the theoretical uncertainty on the strong coupling constant $\alpha_{\text{strong}} = g^2/(4\pi)$ will be crucial in the study of several physical processes in the near future, see, e.g., Ref. [1] for a recent review. In the last two decades, the Lattice Community has spent a huge effort to improve the precision of the determination of the strong coupling [2–9]. As a result, the averaged lattice estimation [10] is now among the most accurate determinations entering the world-average reported in the PDG [11].

From the lattice perspective, determining the strong coupling constant practically amounts to calculate the dynamically-generated scale $\Lambda_{\text{QCD}}$. Thanks to the so-called *decoupling method* [1, 12, 13], this can be in turn traced back to the computation of the confinement scale $\Lambda_{\text{YM}}$ of the pure-gauge theory, i.e., the pure SU(3) gluodynamics with

no dynamical quarks. This quantity has been the target of several lattice calculations in the last 15 years [14–23].

At first glance, the determination of $\Lambda_{\rm YM}$ seems a simpler task compared to the calculation of $\Lambda_{\rm QCD}$, given that pure-Yang–Mills simulations are less computationally-demanding than full QCD ones involving dynamical fermions. However, accurately determining this quantity is a non-trivial numerical challenge, as it requires to keep several sources of systematic errors under control at the sub-percent level. The present paper aims at addressing one of the potentially most serious sources of undesired systematic errors, namely, the strong correlation between the coupling and the topological modes of Yang–Mills theories.

To understand the reason behind this correlation and why it can be an issue, consider the following. A powerful and accurate technique to determine the strong coupling from lattice simulations is to define it from the action density after the gauge fields have been evolved under the gradient flow [24–26]. After the flow, it is well known that the action density becomes highly correlated with the topological background of the underlying gauge field [27]. The topological charge $Q$, in turn, suffers for very large auto-correlation times if the lattice spacing is fine [28–30]. This computational problem, known as *topological freezing*, is due to the loss of ergodicity of standard local updating algorithms close to the continuum limit. Practically, it prevents to correctly sample the topological charge distribution in affordable Monte Carlo simulations. As a matter of fact, when the lattice spacing is sufficiently fine, very few to no fluctuations of $Q$ are observed during typical runs. Given the strong correlation between the topological charge and the action density after the flow, and considering that exploring fine lattices is a necessity to pin down the systematic error related to the continuum limit extrapolation, topological freezing can potentially introduce an undesired bias also in the determination of the strong coupling from the gradient flow, and thus in the $\Lambda$-parameter. So, it is extremely relevant to carefully check if and how topology affects the gradient flow determination of the strong coupling, which is exactly the aim of the present study.

Generally speaking, for what concerns the determination of $\Lambda$, the freezing problem is usually circumvented in lattice computations by defining the coupling through a projection onto the $Q = 0$ topological charge sector [27]. Since in perturbation theory this is the only relevant sector, this definition is expected to amount just to a particular definition of the regularization scheme. Thus, once properly matched to a more customary scheme such as the $\overline{\rm MS}$, this choice should not introduce any systematic in the determination of $\Lambda$. However, *a priori* it is not obvious that, in the presence of topological freezing, fluctuations within each fixed topological sectors are correctly sampled.[1] Moreover, it would be reassuring to explicitly verify in an actual numerical calculation that a non-projected definition of the coupling leads to the same determination of the dynamical scale.

In this paper, we aim exactly at checking in a systematic way what is the impact of topology freezing and topology projection on the determination of the coupling. To this end we will use a novel numerical technique designed to efficiently circumvent topolog-

[1] For a first investigation of this issue in the $2d$ U(1) gauge theory see Ref. [31].

ical freezing, the *Parallel Tempering on Boundary Conditions* (PTBC) algorithm. This algorithm, initially proposed for $2d$ $\mathrm{CP}^{N-1}$ models by M. Hasenbusch [32], and implemented for $4d$ $\mathrm{SU}(N)$ Yang–Mills theories too [33], has been widely employed in the last few years to improve the state of the art of the lattice studies of several topological and non-topological quantities, thanks to the impressive reduction of the auto-correlation time of the topological charge it allows to achieve [33–38].

In a few words, the PTBC algorithm consists in simulating several replicas of the lattice, differing among themselves for the boundary conditions imposed on a handful of gauge links, chosen so as to interpolate among Open Boundary Conditions (OBCs) and Periodic Boundary Conditions (PBCs). All lattice replicas are updated simultaneously and independently, and swaps of gauge configurations among different replicas are proposed during the Monte Carlo. The idea is that a gauge configuration, thanks to the swaps, is able to perform a random walk among the replicas, experiencing different boundary conditions. Since it is well known that simulations with open boundaries suffer for much smaller auto-correlation times [39, 40], this has the beneficial effect of "transferring" the fast decorrelation of the topological charge to the periodic replica, which is where all measures are performed. This last point is a crucial ingredient of the PTBC algorithm, as it allows to circumvent the unphysical effects introduced by OBCs, which require to stay sufficiently far from the boundaries, thus allowing to keep finite size effects under control more easily.

The goal of the present investigation is twofold. First, we aim at comparing the values of the projected coupling obtained with the standard and the PTBC algorithms, in order to explicitly verify whether the former is able to correctly sample gauge configurations within the $Q = 0$ sector regardless of topology freezing. Some preliminary results about this point were presented at the 2023 Lattice conference [41]. Secondly, we aim at verifying that the adoption of a non-projected coupling leads to the same result for the $\Lambda$ parameter. To this end, the most intuitive approach would be to perform the full computation of the dynamical scale with both couplings. However, this method is not ideal as it is difficult to disentangle the possible effects of topology freezing and of topology projection from the other sources of systematic error. Instead, we adopted a more stringent strategy that does not require the full computation of the $\Lambda$-parameter, as it will be explained in the following section.

This manuscript is organized as follows. In Sec. 2 we explain in detail our strategy to check the impact of fixed-topology-projection on the determination of $\Lambda$. In Sec. 3 we present our numerical setup, describing how we implemented the PTBC algorithm in combination with the twisted volume-reduced setup of Ref. [22], and the techniques employed to compute the strong coupling via the gradient flow. In Sec. 4 we discuss our numerical results. Finally, in Sec. 5 we draw our conclusions.

## 2 The $\Lambda$-parameter and the step-scaling method

To better explain the strategy we followed to check the impact of topology projection on the determination of the $\Lambda$-parameter, we recall the definition of this quantity, and how it is computed on the lattice.

The Gell-Mann–Low $\beta$-function defined in the regularization scheme s,

$$\beta_{\rm s}(\lambda_{\rm s}) \equiv \frac{d\lambda_{\rm s}(\mu)}{d\log(\mu^2)} \underset{\lambda_{\rm s}\to 0}{\sim} -\lambda_{\rm s}^2\left(b_0 + b_1\lambda_{\rm s} + b_2^{(\rm s)}\lambda_{\rm s}^2 + \dots\right), \tag{2.1}$$

defines a first-order differential equation which expresses the running of the renormalized SU($N$) 't Hooft coupling $\lambda_{\rm s}(\mu) \equiv N g_{\rm s}^2(\mu)$, and admits a perturbative expansion which is universal (i.e., scheme-independent) up to the 2-loop order. The equation in (2.1) can be exactly integrated, and the scheme-dependent, renormalization-group-invariant, $\Lambda$-parameter is its related integration constant:

$$\frac{\Lambda_{\rm s}}{\mu} = [b_0\lambda_{\rm s}(\mu)]^{-\frac{b_1}{2b_0^2}} e^{-\frac{1}{2b_0\lambda_{\rm s}(\mu)}} \exp\left\{-\int_0^{\lambda_{\rm s}(\mu)} dx \left(\frac{1}{2\beta_{\rm s}(x)} + \frac{1}{2b_0x^2} - \frac{b_1}{2b_0^2x}\right)\right\}. \tag{2.2}$$

Introducing two generic scales $\mu_1$ and $\mu_2$, the following exact relation holds:

$$\frac{\Lambda_{\rm s}}{\mu_1} = \frac{\Lambda_{\rm s}}{\mu_2} \exp\left\{-\int_{\lambda_{\rm s}(\mu_2)}^{\lambda_{\rm s}(\mu_1)} \frac{dx}{2\beta_{\rm s}(x)}\right\}. \tag{2.3}$$

The idea behind the *step-scaling* method [42] is to take $\mu_1 = \mu_{\rm had}$ and $\mu_2 = \mu_{\rm pt}$ sufficiently deep in the non-perturbative and in the perturbative regimes respectively, and to connect these two scales by a sequence of $k$ transformations where, at each step, $\mu$ is increased by a factor of 2: $\mu_{\rm had} \longrightarrow 2\mu_{\rm had} \longrightarrow 2^2\mu_{\rm had} \longrightarrow \dots \longrightarrow 2^k\mu_{\rm had} \equiv \mu_{\rm pt} \gg \mu_{\rm had}$.

The key is that, thanks to step-scaling, the exponential factor appearing in Eq. (2.3) simply becomes:

$$\exp\left\{-\int_{\lambda_{\rm s}(\mu_{\rm pt})}^{\lambda_{\rm s}(\mu_{\rm had})} \frac{dx}{2\beta_{\rm s}(x)}\right\} = \exp\left\{-\int_{\mu_{\rm pt}}^{\mu_{\rm had}} d\log(\mu)\right\} = \frac{\mu_{\rm pt}}{\mu_{\rm had}} = 2^k, \tag{2.4}$$

as $\mu$ changes by a factor of 2 at each step. Then, assuming that $\mu_{\rm pt}$ is sufficiently high that perturbation theory can be trusted, one can evaluate $\Lambda_{\rm s}/\mu_{\rm pt}$ with some perturbative truncation of Eq. (2.2). Since the second factor appearing in Eq. (2.3) is known thanks to the step-scaling procedure, once the low-energy scale $\mu_{\rm had}$ is computed on the lattice, the $\Lambda$-parameter is eventually obtained via:

$$\Lambda_{\rm s} = \left(\frac{\Lambda_s}{\mu_{\rm pt}}\right)\Bigg|_{\rm pt} 2^k\mu_{\rm had}. \tag{2.5}$$

Clearly, to perform the whole step-scaling procedure and determine $\Lambda_{\rm s}$, one needs to compute the strong coupling constant at each step $\lambda_i = \lambda(\mu_i = 2^i\mu_{\rm had})$. As a matter of fact, the high-energy scales that can be typically reached on the lattice are not deep enough in the perturbative regime that perturbation theory alone can be trusted. Thus, what is typically done is to use Eq. (2.4), plus the lattice-determined values of $\lambda_i$, to perform a parametric fit of the unknown higher-order corrections to the known perturbative behavior of the $\beta$-function.

However, for the purpose of checking the impact of topology-projection on $\Lambda_{\rm s}$, it is sufficient to check whether or not the $Q = 0$ projected and the unprojected coupling, which

will of course differ at low energies, lead to the same step-scaling sequence $\mu_{\rm had} \to \mu_{\rm pt}$. Indeed, starting from the same $\mu_{\rm had}$, if the step-scaling passes through the same energy scales $\mu_i = 2^i \mu_{\rm had}$, it will yield for both couplings the same $2^k$ factor in Eq. (2.5). Since also the factor of $\Lambda/\mu_{\rm pt}$ appearing in Eq. (2.5) will be the same, because the two couplings are expected to become exactly equal in the high-energy limit, when the contribution of topological sectors becomes irrelevant, then the two definitions of the coupling will yield the same $\Lambda$-parameter. The pleasant consequence of this observation is that, to check that the two couplings give the same step-scaling chain, it is sufficient to just perform the calculation of the coupling in the first step of the sequence: $\mu_{\rm had} \to 2\mu_{\rm had}$.[2] This is a much more stringent test than performing the whole calculation of $\Lambda$, as it precisely allows to disentangle any possible systematic coming from topology from the other sources of uncertainty.

To run the energy scale $\mu$ on the lattice, it is convenient to work in a scheme where this is taken to be proportional to the inverse lattice size (in physical units): $\mu \propto 1/l$. This approach is very powerful because it allows to exploit finite-size effects at one's own advantage. In order to determine the running $\lambda(\mu)$ for one step of the step-scaling sequence, we practically follow these steps [42]:

1. We consider several simulations points with different values of the lattice extent $L = l/a$ (with $a$ the lattice spacing) with constant $l$, and we define a Line of Constant Physics (LCP) by tuning the bare coupling for each lattice to achieve the same value of the renormalized coupling $\lambda_1 = \lambda(\mu_1)$, with $\mu_1 = 1/(cl)$, with $c$ some $O(1)$ proportionality constant. Clearly, given the 1-to-1 correspondence between $\lambda$ and $\mu$ (i.e., $l$), this is equivalent to tune the bare couplings so as to achieve a fixed value of the lattice size $l$.

2. We calculate the renormalized coupling for the same values of the bare coupling, but doubling the lattice size $L \to 2L$. In principle, one expects these simulations points to approximately constitute a LCP for the renormalized coupling up to lattice artifacts, since the lattice size in physical units is constant and equal to $2l$. Assuming there is a 1-to-1 correspondence between the renormalized coupling and the renormalization scale $\mu$, the value of the coupling $\lambda_0 = \lambda(\mu_0 = \mu_1/2)$ will be defined from the continuum extrapolation of the results obtained on these ensembles.

Clearly, by iterating these 2 steps $k$ times, we achieve the complete step-scaling sequence, but, as we outlined earlier, for our purpose it will be sufficient to just perform them once. As a matter of fact, in order to verify that the $Q = 0$ projected, $\lambda^{(0)}$, and the unprojected coupling, $\lambda^{(\rm noproj)}$, lead to the same step-scaling sequence, and thus to the same dynamical scale, it is sufficient to perform the following check:

$$\exp\left\{-\int_{\lambda^{(0)}(\mu)}^{\lambda^{(0)}(\mu/2)} \frac{dx}{2\beta_0(x)}\right\} = \exp\left\{-\int_{\lambda^{(\rm noproj)}(\mu)}^{\lambda^{(\rm noproj)}(\mu/2)} \frac{dx}{2\beta_{\rm noproj}(x)}\right\}, \tag{2.6}$$

[2] We thank Alberto Ramos for pointing this out.

i.e., our goal is to check that, assuming that the projected coupling allows to correctly define LCPs to realize the step $\mu/2 \to \mu$, these also remain LCPs for the non-projected one, as this guarantees that the same step-scaling sequence is obtained from both couplings. How this check is performed in practice will be explained in more details in Sec. 4.

## 3 Numerical methods

In this section, we describe our numerical setup, namely, the lattice discretization adopted for the gauge action, the strong coupling and the topological charge, and the practical implementation of the PTBC algorithm we employed.

### 3.1 Twisted volume reduction and twisted gradient flow coupling

Concerning the lattice definition of the action and the observables, we follow the same numerical setup of Ref. [22], which we shortly review in this section.

We discretize the pure-gauge SU(3) theory using the Wilson plaquette action on a lattice with lattice spacing $a$, geometry $L^2 \times \tilde{L}^2$, with $\tilde{L} = L/N = L/3$, and Twisted Boundary Conditions (TBCs) along the short directions [43, 44]. These two latter peculiar choices will be better justified shortly. In practice, the discretized action reads:

$$S_{\mathrm{W}}[U] = -Nb \sum_{x,\mu>\nu} Z^*_{\mu\nu}(x) \Re\mathrm{Tr}\left[P_{\mu\nu}(x)\right], \tag{3.1}$$

where $b = 1/\lambda_L$ is the inverse bare 't Hooft coupling and $P_{\mu\nu}(x) = U_\mu(x)U_\nu(x+a\hat{\mu})U^\dagger_\mu(x+a\hat{\nu})U^\dagger_\nu(x)$ is the plaquette operator on site $x$ along the $(\mu,\nu)$ plane. Finally, the factor $Z_{\mu\nu}(x)$ is used to easily impose TBCs for some plaquettes lying along the short plane:

$$Z_{\mu\nu}(x) = Z^*_{\nu\mu}(x) = \begin{cases} e^{i2\pi/3}, & \text{if } (\mu,\nu) = (1,2) \text{ and } x_\mu = x_\nu = 0, \\ 1, & \text{elsewhere.} \end{cases} \tag{3.2}$$

The choice of a lattice with reduced extents along the twisted plane is rooted on the idea of *twisted volume reduction* [45–47] (see also Refs. [48, 49] for reviews on the topic), which is a technique usually employed to study the large-$N$ limit of SU($N$) gauge theories. In the large-$N$ limit, indeed, it has been long known, starting from the seminal paper of Eguchi and Kawai [50], that SU($N$) Yang–Mills theories enjoy a dynamical equivalence between color and space-time degrees of freedom, leading for $N = \infty$ to a volume-independence of the theory. While this property strictly speaking holds true only in the large-$N$ limit, at finite values of $N$ the presence of TBCs allows to achieve en effective increase in the lattice size: $V_{\mathrm{eff}} = N^2 V$. Since our lattice has $V = L^2 \times \tilde{L}^2 = L^4/N^2$, this means that $V_{\mathrm{eff}} = N^2 V = L^4$, i.e., we achieve the same dynamics of a standard hypercubic lattice with size $L$. Adopting TBCs has also several advantages over fully periodic ones: it allows an analytic expansion in the coupling in perturbation theory as opposed to PBCs [51], and it is free of $O(a)$ effects presents, for instance, in the Schrödinger Functional scheme [52].

For what concerns the definition of the renormalized coupling, we make use of the gradient flow, a smoothing procedure that evolves the gauge fields according to the flow-time equations:

$$\partial_t B_\mu(x,t) = D_\nu F_{\nu\mu}(x,t), \quad B_\mu(x,t=0) = A_\mu(x), \tag{3.3}$$

where $D_\mu$ and $F_{\mu\nu}$ stand for the covariant derivative and field strength tensor of the flowed fields. Given that the gradient flow introduces an additional length scale in the game, the *smoothing radius* $r_s = \sqrt{8t}$, with $t$ the flow time in physical units, it is natural in this setup to identify the inverse of this scale as the energy scale $\mu$ of the running coupling. In turn, as already pointed out in Sec. 2, it is natural to choose this length scale as a fraction $c$ of the physical size of the lattice. When combined with our asymmetric volume setup and twisted boundary conditions, the gradient flow leads to a particular scheme to define the coupling known as *Twisted Gradient Flow* (TGF) [22, 53, 54]. In more concrete terms, the TGF renormalized coupling is defined in the continuum theory according to:

$$\lambda_{\rm TGF}\left(\mu = \frac{1}{cl}\right) = \mathcal{N}(c)\,\langle t^2 E(t)\rangle\Big|_{\sqrt{8t}=cl}, \tag{3.4}$$

with $E(t)$ the energy density evaluated on the flowed fields:

$$E(t) = \frac{1}{2}{\rm Tr}\left\{F_{\mu\nu}(x,t)F_{\mu\nu}(x,t)\right\}, \tag{3.5}$$

and with $\mathcal{N}(c)$ a normalization factor given by:

$$\mathcal{N}(c) = \frac{128\pi^2}{3N\mathcal{A}(\pi c^2)}, \tag{3.6}$$

$$\mathcal{A}(x) = x^2\theta_3^2(0,ix)\left[\theta_3^2(0,ix) - \theta_3^2(0,ixN^2)\right], \tag{3.7}$$

with $\theta_3(z,ix) = x^{-1/2}\sum_{m\in\mathbb{Z}}\exp(-\pi(x-z)^2/x)$ the Jacobi $\theta_3$ function, which is introduced to ensure that, at lowest order of perturbation theory, $\lambda_{\rm TGF} = \lambda_{\overline{\rm MS}} + O(\lambda^2_{\overline{\rm MS}})$. The value of $c$ can be freely chosen, and just amounts to define a particular regularization scheme; here we adopt $c = 0.3$. Although we will not use it here, we also recall that the conversion factor between the $\Lambda$-parameters in the TGF and in the $\overline{\rm MS}$ scheme is known [22].

As mentioned in the introduction, it is customary to address the issue of topology freezing by projecting the determination of the coupling into the sector of configurations with zero topological charge [27] as follows:

$$\lambda^{(n)}_{\rm TGF}\left(\mu = \frac{1}{cl}\right) = \frac{128\pi^2 t^2}{3N\mathcal{A}(\pi c^2)}\frac{\langle E(t)\,\delta(Q-n)\rangle}{\langle\delta(Q-n)\rangle}\Bigg|_{\sqrt{8t}=cl}, \tag{3.8}$$

$$Q = \frac{1}{32\pi^2}\varepsilon_{\mu\nu\rho\sigma}\int d^4x\,{\rm Tr}\left\{F_{\mu\nu}(x)F_{\rho\sigma}(x)\right\} \in \mathbb{Z}, \tag{3.9}$$

where $\delta(Q-n)$ stands for a $\delta$-function that restricts the calculation to configurations with topological charge $Q = n$. The unprojected coupling in Eq. (3.4), averaged over all topological sectors, will be referred to in the following as $\lambda^{\rm (noproj)}_{\rm TGF}$.

On the lattice, we use the Wilson flow combined with twisted boundary conditions to determine the coupling, meaning that the gauge fields are evolved during the flow using exactly the action in Eq. (3.1). As for the energy density, we used the clover-discretized energy density given by:

$$E_{\rm clov}(t) = \frac{1}{12NL^2\tilde{L}^2}\sum_{\mu>\nu}\sum_x \mathrm{Tr}\left[C_{\mu\nu}(x,t)C_{\mu\nu}(x,t)\right], \tag{3.10}$$

with $C_{\mu\nu}(x,t)$ the clover operator in the site $x$ along the $(\mu,\nu)$ plane,

$$\begin{aligned} C_{\mu\nu}(x,t) \;=\; & \frac{1}{4}\Im[Z^*_{\mu\nu}(x)P_{\mu\nu}(x,t) + Z^*_{\mu\nu}(x-a\hat{\nu})P_{-\nu\mu}(x,t) \\ & + Z^*_{\mu\nu}(x-a\hat{\mu})P_{\nu-\mu}(x,t) + Z^*_{\mu\nu}(x-a\hat{\mu}-a\hat{\nu})P_{-\mu-\nu}(x,t)], \end{aligned} \tag{3.11}$$

where $U_{-\mu}(x) = U^\dagger_\mu(x-a\hat{\mu})$. In order to eliminate the leading lattice artefacts in perturbation theory for the Wilson flow, we also take a discretized version of the normalization constant $\mathcal{N}$:

$$\mathcal{N}_L^{-1}(c,L) \;=\; \frac{c^4}{128}\sum_{\mu\neq\nu}\sum_q{}' e^{-\frac{1}{4}c^2L^2\hat{q}^2}\frac{1}{\hat{q}^2}\sin^2(q_\nu)\cos^2(q_\mu/2), \tag{3.12}$$

where $\hat{q}_\mu = 2\sin(q_\mu/2)$ stands for the lattice momentum, with $q_\mu = 2\pi n_\mu/L$, $n_\mu = 0,\cdots,L-1$, and with the prime in the sum denoting the exclusion of momenta with both components in the twisted plane satisfying $Lq_i \propto 2N\pi = 6\pi$.

The TGF technique will be also used to define the topological charge on the lattice. In particular, we will adopt the simplest parity-defined clover discretization,

$$Q_{\rm clov} = \frac{1}{32\pi^2}\sum_x\sum_{\mu,\nu,\rho,\sigma}\varepsilon_{\mu\nu\rho\sigma}\mathrm{Tr}\left[C_{\mu\nu}(x)C_{\rho\sigma}(x)\right], \tag{3.13}$$

and define our physical topological charge and topological susceptibility after the flow, at the same flow time employed to define the coupling:

$$Q = Q_{\rm clov}(\sqrt{8t}=cl), \qquad\qquad a^4\chi = \frac{\langle Q^2\rangle}{\tilde{L}^2L^2}. \tag{3.14}$$

In our simulations, this amount of flow turned out to be in all cases well within the observed plateau in $Q$ as a function of $t$ for large enough flow times, and the flowed clover charge at $\sqrt{8t}=cl$ always turned out to be extremely close to an integer number. Therefore, one can safely define the projected coupling onto the topological sector $Q=n$ as follows:

$$\lambda^{(n)}_{\rm TGF}\left(\mu=\frac{1}{cl}\right) = \mathcal{N}_L(c,L)\frac{\langle t^2E_{\rm clov}(t)\hat{\delta}(Q-n)\rangle}{\langle\hat{\delta}(Q-n)\rangle}\Bigg|_{\sqrt{8t}=cl}, \tag{3.15}$$

where

$$\hat{\delta}(Q-n) = \begin{cases} 1, & |Q-n|<0.5 \\ 0, & \text{otherwise.} \end{cases} \tag{3.16}$$

### 3.2 The PTBC algorithm in the presence of twisted boundary conditions

In order to circumvent topological freezing for fine lattice spacings, we adopt the SU($N$) PTBC algorithm of Ref. [33], which can be easily generalized to the current setup with TBCs. In practice, we consider $N_r$ replicas of the lattice, each one differing for the boundary conditions imposed on a small sub-region, which in the following will be addressed as *the defect*. In this work, we choose the defect $D$ to be an $L_d \times L_d \times L_d$ cube, and place it on the time boundary, so that no plaquette affected by the twist has links that cross $D$ orthogonally. This way, the tempering will always affect links that, in the physical replica (i.e., the one on which observables are computed), enjoy PBCs. Concerning the unphysical replicas, the idea is to choose their boundary conditions on the defect in such a way to interpolate between PBCs and OBCs. This can in practice be easily achieved by taking the action of the replica $r$ of the form:

$$S_{\mathrm{W}}^{(r)}[U_r] = -Nb \sum_{x,\mu>\nu} K_{\mu\nu}^{(r)}(x) Z_{\mu\nu}^{*}(x) \Re\mathrm{Tr}\left[P_{\mu\nu}^{(r)}(x)\right], \tag{3.17}$$

where $U_r$ denotes the gauge links of the replica $r$, and where the factor $K_{\mu\nu}^{(r)}(x)$, which comes attached to each plaquette, is used to change the boundary conditions on the defect, similarly to the action of the twist factor $Z_{\mu\nu}(x)$:

$$K_{\mu\nu}^{(r)}(x) \equiv K_{\mu}^{(r)}(x) K_{\nu}^{(r)}(x + a\hat{\mu}) K_{\mu}^{(r)}(x + a\hat{\nu}) K_{\nu}^{(r)}(x), \tag{3.18}$$

$$K_{\mu}^{(r)}(x) \equiv \begin{cases} c(r), & \mu = 0, \quad x_0 = L - 1, \quad 0 \leq x_1, x_2, x_3 < L_d \\ 1, & \text{elsewhere}, \end{cases} \tag{3.19}$$

with $0 \leq c(r) \leq 1$, where the edge cases 0 and 1 correspond, respectively, to open and periodic boundaries. In the following, all observables will be computed in the physical replica $r = 0$ with $c(r = 0) = 1$.

For what concerns the Monte Carlo PTBC sampling algorithm, each replica is updated simultaneously and independently by performing 1 lattice sweep of the standard local heat-bath algorithm [55, 56], followed by $n_{\mathrm{ov}}$ lattice sweeps of the standard local over-relaxation algorithm [57]. Then swaps among two adjacent replicas $(r, s = r + 1)$ are proposed, and accepted via a standard Metropolis step:

$$p(r, s) = \min\left\{1, e^{-\Delta S_{\mathrm{swap}}^{(r,s)}}\right\}, \tag{3.20}$$

$$\Delta S_{\mathrm{swap}}^{(r,s)} = S_{\mathrm{W}}^{(r)}[U_s] + S_{\mathrm{W}}^{(s)}[U_r] - S_{\mathrm{W}}^{(r)}[U_r] - S_{\mathrm{W}}^{(s)}[U_s]. \tag{3.21}$$

Note that, for the purpose of calculating $\Delta S_{\mathrm{swap}}^{(r,s)}$, one does not need to iterate over the whole lattice, as the only non-vanishing contributions to it come from the links found at most at a one lattice spacing distance from the defect. Given that the optimal setup is achieved when the mean acceptances $\mathcal{P}_r \equiv \langle p(r, r + 1)\rangle$ are roughly constant, so that a given configuration can perform a sort of random walk among different replicas, we performed short test runs

in order to tune the $c(r)$ tempering parameters in order to achieve $\mathcal{P}_r \approx \mathcal{P} \approx 20\%$. With this choice, the number of replicas necessary to achieve a given constant mean acceptance $\mathcal{P}$ becomes just a function of the defect size in lattice units $L_d$.

Between two full updating sweeps involving the whole lattice, we performed several hierarchical updates on small sub-lattices centered around the defect, in order to update more frequently the links with tempered boundary conditions. This is done to improve the efficiency of the algorithm, as this is the region where new topological excitations are more likely to be created/destroyed. Moreover, after each swap is proposed, we translate the links of the periodic replica by one lattice spacing in a random direction, moving also consistently the position of the twisted plaquettes. This step is done to effectively move the position of the defect around the lattice, which is expected to improve the efficiency of the algorithm, as in this way topological excitations are created/destroyed in different space-time points.

In a few words, given that the numerical effort required by hierarchical udpates, translations and swaps is negligible compared to the full sweeps of the lattice, one full parallel tempering updating step requires a numerical effort which is of the order of $N_r \times n_{\rm ov}$. This observation will be crucial to compare the efficiency of this algorithm with the standard one.

## 4 Results

This section is devoted to discuss the impact of topology on the determination of the strong coupling by comparing results obtained using the standard and the PTBC algorithms. Following the strategy described in Sec. 2, we aim at performing the first step in the scaling sequence connecting $\mu_{\rm had}$ with $2\mu_{\rm had}$ using both the projected and unprojected couplings, as determined with PTBC and with the standard algorithms. This first step reproduces the one used in Ref. [22] to determine the $\Lambda$-parameter. The idea is the following:

(A) First, using simulations performed with the standard algorithm, we select the bare couplings $b$ so as to have an approximately fixed value of the $Q = 0$ projected coupling $\lambda^{(0)}_{\rm TGF}(2\mu_{\rm had})$ on the $L = 12, 18, 24$ lattices.[3] Assuming that this algorithm samples correctly the $Q = 0$ sector, this set corresponds to a LCP with fixed physical volume $l = aL \simeq 0.55$ fm, which we dub LCP1. Then, we perform simulations for these very same values of $b$, but on doubled lattices with sizes $L = 24, 36, 48$. The corresponding values of the lattice step scaling functions, extrapolated to the continuum limit, give $\lambda^{(0)}_{\rm TGF}(\mu_{\rm had})$. These results are discussed in Sec. 4.1.

(B) Finally, on lattices with $L = 24, 36, 48$, we determine the bare couplings $b$ for which the $Q = 0$ projected coupling takes the value $\lambda^{(0)}_{\rm TGF}(\mu_{\rm had})$ determined in (A); details on how to do the tuning are provided in Ref. [22]. This last set of simulation points should correspond to a LCP with fixed physical volume $l = aL = 1/\mu_{\rm had} \sim 1.1$ fm,

[3] A possible small mismatch in the target couplings can be easily corrected for later on, as will be described in Sec. 4.2.

| LCP1 ($l = 0.55$ fm) | | | | | | Scale setting | |
|---|---|---|---|---|---|---|---|
| $L$ | $3 \times b$ | $N_r$ | $L_d$ | $n_{\rm ov}^{\rm (PTBC)}$ | $n_{\rm ov}^{\rm (std)}$ | $\beta$ | $a/\sqrt{t_0}$ |
| 12 | 6.4881 | 10 | 2 | 12 | 12 | 6.4881 | 0.2770(35) |
| 18 | 6.7790 | 17 | 3 | 12 | 18 | 6.7790 | 0.1846(24) |
| 24 | 7.0000 | 24 | 4 | 12 | 24 | 7.0000 | 0.1385(18) |

| LCP1 with doubled $L$ | | | | | | LCP2 ($l = 1.1$ fm) | | | | | |
|---|---|---|---|---|---|---|---|---|---|---|---|
| $L$ | $3 \times b$ | $N_r$ | $L_d$ | $n_{\rm ov}^{\rm (PTBC)}$ | $n_{\rm ov}^{\rm (std)}$ | $L$ | $3 \times b$ | $N_r$ | $L_d$ | $n_{\rm ov}^{\rm (PTBC)}$ | $n_{\rm ov}^{\rm (std)}$ |
| 24 | 6.4881 | 18 | 4 | 12 | 24 | 24 | 6.459 | 18 | 4 | 12 | 24 |
| 36 | 6.7790 | 34 | 6 | 12 | 36 | 36 | 6.765 | 34 | 6 | 12 | 36 |
| 48 | 7.0000 | 54 | 8 | 12 | 48 | 48 | 6.992 | 54 | 8 | 12 | 48 |

**Table 1**. Summary of simulation parameters, where the number of replicas $N_r$ and the defect size $L_d$ only refer to runs with the PTBC algorithm. The numbers $n_{\rm ov}^{\rm (PTBC)}$ and $n_{\rm ov}^{\rm (std)}$ refer to the number of over-relaxation lattice sweep per over-heat lattice sweep for, respectively, the PTBC and the standard algorithm. The scale setting was taken from Refs. [58–60] or from a spline interpolation of data thereof. The defect size in lattice units $L_d$ was scaled in order to keep its length constant in physical units: $L_d/L = 1/6$. The number of replicas was scaled as a function of $L_d$ in order to achieve in all cases an almost uniform swap acceptance rate of $\sim 20\%$ among adjacent replicas.

which we dub as LCP2. These simulations, whose results will be used to assess the impact of topology freezing and topology projection on the step-scaling sequence $\mu_{\rm had} \to 2\mu_{\rm had}$, are discussed in Sec. 4.2.

All the simulations outlined in (A) and (B) will be performed both with the standard and the PTBC algorithms. All simulation parameters are summarized in Tab. 1, where we also report the employed scale setting, which in this paper was done using the standard gradient flow scale $t_0$ [58]. For brevity, we moved all obtained lattice results in App. A.

Concerning simulations with parallel tempering, following the prescription advocated in the original references [32, 33], we kept the defect size fixed in physical units as we approached the continuum limit. This of course requires to scale the defect size $L_d$ as $1/a$. Since we also kept the mean acceptance swap rate fixed to $\approx 20\%$ for each adjacent replica couple (cf. Fig. 1), the number of replicas $N_r$ is just a function of $L_d$, and is empirically found to scale approximately as $N_r \sim L_d^{3/2} \sim 1/a^{3/2}$, in agreement with the findings of Refs. [32, 33]. As already pointed out in the previous section, the numerical cost of one parallel tempering updating step is of the order of $N_r \times n_{\rm ov}^{\rm (PTBC)}$, while the computational cost of one standard updating step is of the order of $n_{\rm ov}^{\rm (std)}$, where $n_{\rm ov}$ stands for the number of over-relaxation lattice sweeps per heat-bath lattice sweep. Thus, in the following, it will be more convenient to just compare the two algorithms expressing their Monte Carlo times in terms of a common scale, the number of lattice sweeps $n_{\rm sweeps} = N_r \times n_{\rm ov} \times n_{\rm steps}$, with $n_{\rm steps}$ the number of updating steps (of course $N_r = 1$ for the standard algorithm).

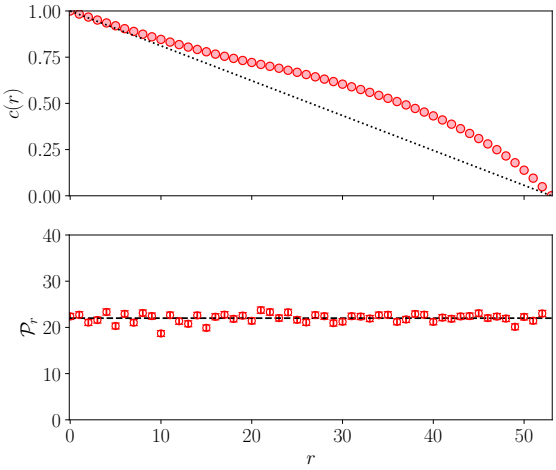


**Figure 1**. Figure refers to the PTBC run with $L = 48$, $3b = 6.992$, $N_r = 48$, $L_d = 8$. Top panel: tuned values of $c(r)$ compared with a simple linear behavior $c(r) = 1 - r/(N_r - 1)$. Bottom panel: corresponding mean swap acceptance rates $\mathcal{P}_r = \langle p(r, r+1)\rangle \approx 22(2)\%$.

### 4.1 Impact of topology projection on the strong coupling

We start our investigation from the LCP1, where the values of the bare couplings were chosen in Ref. [22] to achieve an approximately constant value of the projected coupling $\lambda^{(0)}_{\rm TGF} \approx 13.93(5)$. This corresponds to an almost constant lattice size $l = aL \sim 0.55$ fm, and to an energy scale $\mu = 2\mu_{\rm had} = 1/(cl) = 1/(0.3l) \sim 1.2$ GeV.

Since in the thermodynamic limit the topological susceptibility of the pure SU(3) gauge theory is $t_0^2\chi = 6.67(4)\cdot 10^{-4}$ [61], and since for our simulations points $l/\sqrt{t_0} \simeq 3.32$, we can set the following (very loose) upper bound for these runs: $\langle Q^2\rangle \lesssim \tilde{l}^2 l^2 \chi = (l/\sqrt{t_0})^4 t_0^2 \chi/N^2 \sim 0.009 \ll 1$. This means that in this case topological fluctuations are not only inhibited by topology freezing, i.e., by the loss of ergodicity of the updating algorithm on fine lattices, but they are also strongly suppressed by the smallness of the lattice volume, which yields a very small value of $\langle Q^2\rangle$, i.e., of the variance of the topological charge distribution. More precisely, assuming $P_0 \gg P_1 \gg P_2 \gg \ldots$, where $P_n$ is the probability of visiting the topological sector with $Q = n$, and using that $P_{-n} = P_n$, the following approximation

$$\langle Q^2\rangle \simeq \frac{2P_1 + \ldots}{P_0 + 2P_1 + \ldots} \simeq \frac{2P_1}{P_0} \lesssim 9\cdot 10^{-3} \tag{4.1}$$

shows that we can expect the probability of visiting the topological sector with $|Q| = 1$ to be at least two orders of magnitude smaller than the probability of visiting $Q = 0$. This problem is well known in the finite-temperature QCD literature, as sufficiently above the QCD chiral crossover $T_c \simeq 155$ MeV the topological susceptibility is rapidly suppressed as $\chi \sim (T/T_c)^{-8}$ [62–70], meaning that, on typically-employed volumes and for sufficiently large temperatures, $\langle Q^2\rangle = V\chi \ll 1$, as in the present case.

Being the damping of topological fluctuations in this case mainly due to a physical dynamical effect, and not to a consequence of topology freezing, we expect to see a small number of topological fluctuations even when running with the parallel tempering. More-

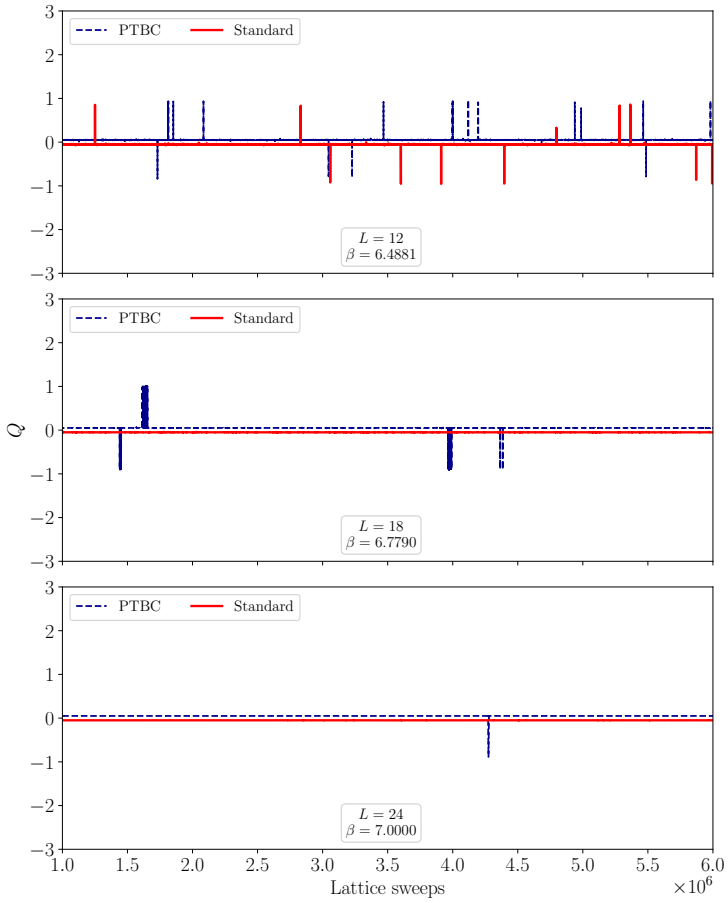


**Figure 2**. Comparison of the Monte Carlo evolutions of the topological charge obtained with the standard and the PTBC algorithm for the 3 simulations points corresponding to a LCP with fixed lattice size $l \simeq 0.55$ fm and fixed projected coupling $\lambda_{\rm TGF}^{(0)} \approx 13.93(5)$. In both cases, the horizontal Monte Carlo time was expressed in units of lattice sweeps in order to make a fair comparison among the two algorithms. This means that the number of updating steps in both cases was multiplied by the number of over-relaxation sweeps per heat-bath sweep, $n_{\rm ov}$, and, in the case of PTBC, also by the number of replicas $N_r$.

over, one also expects $\lambda_{\rm TGF}^{(0)} \simeq \lambda_{\rm TGF}^{(\rm noproj)}$, given that the contribution from higher-charge sectors is very suppressed.[4] This is perfectly reasonable, as in our setup smaller volumes mean larger energy scales, and closer to the perturbative regime we expect the $Q = 0$ sector to largely dominate over the others.

Our expectations are fully confirmed by our results for the Monte Carlo evolution of the flowed lattice topological charge, shown in Fig. 2, as well as those obtained for the coupling, shown in Fig. 3. As it can be observed, the Monte Carlo evolutions of the topological charge

[4] Actually, to definitively conclude that $\lambda_{\rm TGF}^{(0)} \simeq \lambda_{\rm TGF}^{(\rm noproj)}$, in principle one should also check that $\lambda_{\rm TGF}^{(0)}/\lambda_{\rm TGF}^{(1)} \gg P_1/P_0$, which we are currently unable to do with the current setup for these simulation points with small volumes, as we cannot reliably measure $\lambda_{\rm TGF}^{(1)}$. To this end, one should employ one of the several strategies that have been devised in the literature to sample rare events, such as the multicanonic algorithm [66, 67, 70, 71], or the density of states method [69, 72].

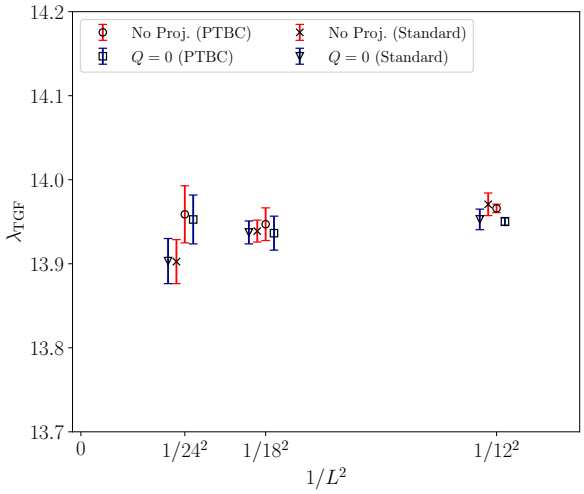


**Figure 3**. Comparison of the $Q = 0$ projected and unprojected couplings obtained with the standard algorithm in Ref. [22] with those obtained in the present work with the PTBC algorithm for the 3 simulations points corresponding to a LCP with $l = 0.55$ fm, tuned to achieve a constant value of $\lambda^{(0)}_{\rm TGF}$.

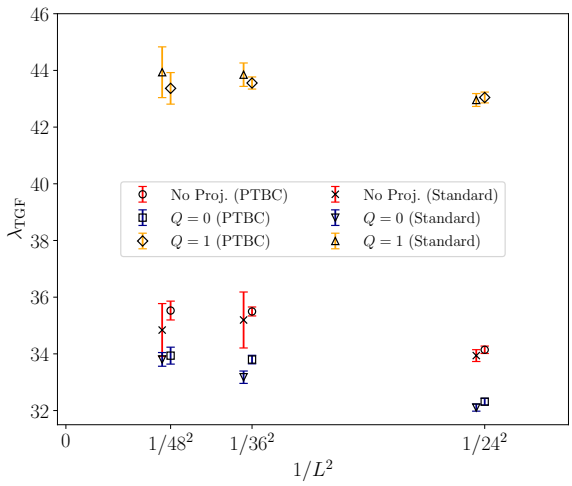


**Figure 4**. Comparison of the $Q = 0$ projected and unprojected couplings obtained with the standard algorithm and the PTBC algorithm for the 3 simulations points corresponding to the same bare couplings of the LCP with $l = 0.55$ fm, but on lattices with doubled sizes.

are very look-alike with both algorithms, as the suppression of topological fluctuations has a physical origin, and the $Q = 0$ sector dominates the actual topological charge distribution. This of course means that no difference can be appreciated between the $Q = 0$ projected and the unprojected couplings. As a matter of fact, in all cases we observe at most differences at the level of one standard deviation within the per mil accuracy with which we have determined the coupling. We thus conclude that, for the purpose of calibrating the LCP, both the projected and the unprojected coupling lead to perfectly consistent results.

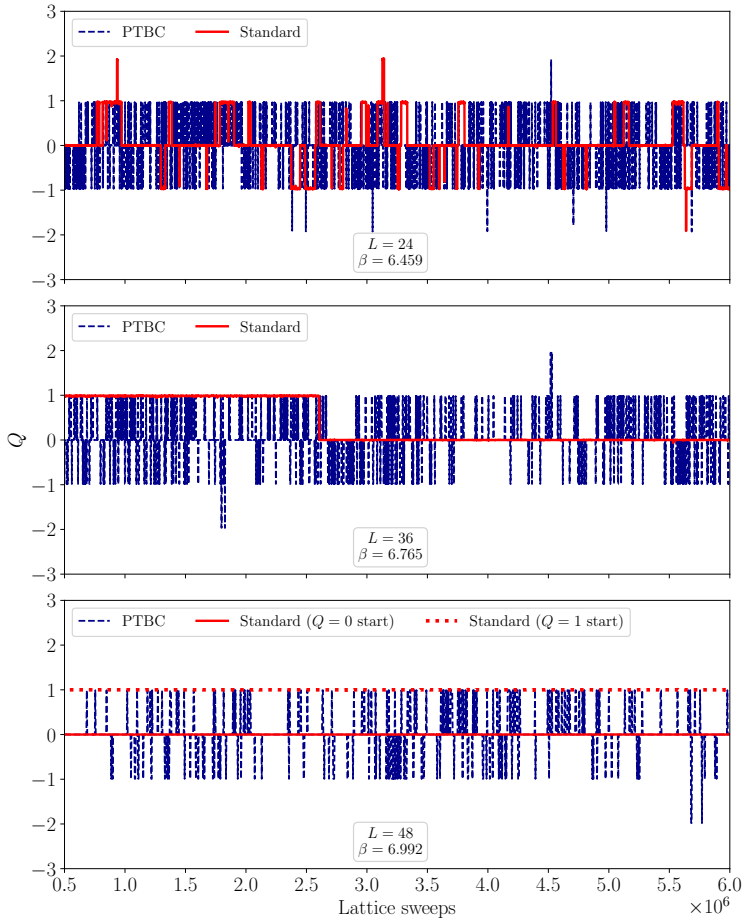


**Figure 5**. Comparison of the Monte Carlo evolutions of the topological charge obtained with the standard and the PTBC algorithm for the 3 simulations points corresponding to a LCP with $l = 1.1$ fm. In both cases, the horizontal Monte Carlo time was expressed in units of lattice sweeps in order to make a fair comparison among the two algorithms. This means that the number of updating steps in both cases was multiplied by the number of over-relaxation sweeps per heat-bath sweep, $n_{\rm ov}$, and, in the case of PTBC, also by the number of replicas $N_r$.

We now move to the computation of the lattice step-scaling function $\lambda_{\rm TGF}(\mu_{\rm had})\Big|_{\lambda_{\rm TGF}(2\mu_{\rm had})}$ using the same bare couplings of LCP1 on the doubled lattices. Given that we have now doubled the lattice sizes, we expect $\langle Q^2\rangle \sim O(0.1)$, thus we foresee topological fluctuations to start to become important. This in turn implies that $\lambda_{\rm TGF}^{\rm (noproj)}$ and $\lambda_{\rm TGF}^{(0)}$ now will differ sizably. Results for the projected and the unprojected couplings, obtained both with the PTBC and the standard algorithms, are shown in Fig. 4. As expected, we now observe a sizeable difference between the projected and the unprojected couplings, due to the contribution of higher-charge sectors, which are now much less suppressed. However, concerning the projected couplings, we observe that the results obtained with the standard algorithms are in perfect agreement with those obtained with PTBC, as at most we observe $1-2$ standard deviation differences within our per mil accuracy. This is a very non-trivial check

| Parallel Tempering | | | | | |
|---|---|---|---|---|---|
| $L$ | $3 \times b$ | $\tau\left(\lambda_{\rm TGF}^{(0)}\right)$ | $\tau\left(\lambda_{\rm TGF}^{(1)}\right)$ | $\tau\left(\lambda_{\rm TGF}^{(\rm noproj)}\right)$ | $\tau\left(Q^2\right)$ |
| 24 | 6.459 | 260(65) | 156(26) | 1040(260) | 1430(260) |
| 36 | 6.765 | 980(250) | 610(120) | 4200(1100) | 7350(2500) |
| 48 | 6.992 | 1950(580) | 1170(390) | 11700(4700) | 31100(11700) |

| Standard | | | | | |
|---|---|---|---|---|---|
| $L$ | $3 \times b$ | $\tau\left(\lambda_{\rm TGF}^{(0)}\right)$ | $\tau\left(\lambda_{\rm TGF}^{(1)}\right)$ | $\tau\left(\lambda_{\rm TGF}^{(\rm noproj)}\right)$ | $\tau\left(Q^2\right)$ |
| 24 | 6.459 | 800(120) | 288(58) | 5760(1150) | 20200(2900) |
| 36 | 6.765 | 2070(450) | 840(320) | $1.10(32)\cdot 10^5$ | $5.1(1.5)\cdot 10^5$ |
| 48 | 6.992 | 4600(1200) | 2300(580) | $\gtrsim 5.8(2.4)\cdot 10^6$ | $\gtrsim 5.8(2.4)\cdot 10^6$ |

**Table 2**. Integrated auto-correlation time, obtained from a standard binned jack-knife analysis, of the projected and unprojected definitions of the couplings, and of the squared topological charge, obtained with the standard and the PTBC algorithm for the 3 simulations points corresponding to a LCP with $l = 1.1$ fm. For the finest lattice spacing explored, only an upper bound on the auto-correlation time of $Q^2$ and of $\lambda_{\rm TGF}^{(\rm noproj)}$ could be set for the simulation with the standard algorithm, since no fluctuation of the topological charge was observed. In both cases, the auto-correlation time was expressed in units of lattice sweeps in order to make a fair comparison among the two algorithms. This means that the auto-correlation time was in both cases multiplied by the number of over-relaxation sweeps per heat-bath sweep, $n_{\rm ov}$, and, in the case of PTBC, also by the number of replicas $N_r$.

that projection works even in the presence of severe topological freezing.

Finally, let us conclude our discussion by comparing the performances of the standard and the PTBC algorithms. For that we will use long-run simulations performed on the lattice corresponding to the LCP2 in Tab. 1. While the standard algorithm exhibits significant topological freezing, especially at the two finest lattice spacings explored, the PTBC one allows to achieve an impressive improvement in the observed number of topological fluctuations at fixed parameters. Such improvement can be clearly seen by inspecting Fig. 5, where we compare the Monte Carlo evolutions of $Q$ obtained with the two algorithms, after expressing the Monte Carlo time in the same units in both cases. Note that for the finest lattice spacing we observed no fluctuations of $Q$ with the standard algorithm, and two independent stories started from configurations with $Q = 0$ and $Q = 1$ both remained stuck in the initial topological sector.

The algorithmic improvement obtained with PTBC can be quantified from the comparison of the obtained auto-correlation times, again expressed in terms of number of lattice sweeps in order to keep into account the different number of over-relaxation sweeps per heat-bath sweeps used in the two cases, as well as the numerical over-head introduced by the simulation of the unphysical replicas. Numerical results are reported in Tab. 2, and shown in Fig. 6. For what concerns the squared topological charge, we observe a reduction of the auto-correlation time $\tau$ by more than one order of magnitude for the coarsest

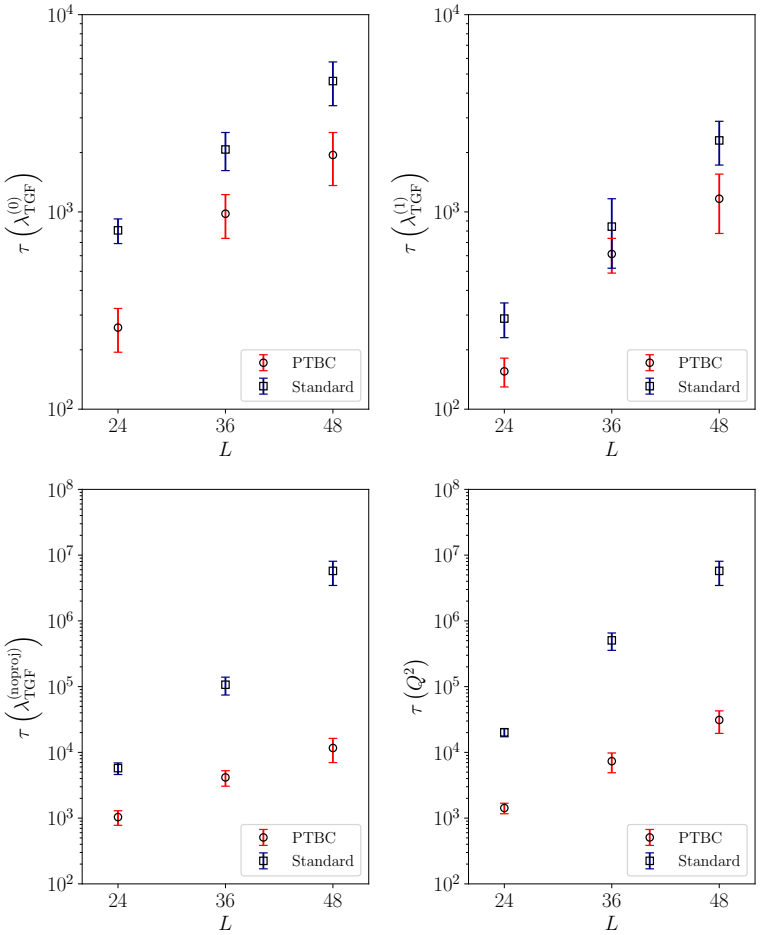


**Figure 6**. Comparison of the integrated auto-correlation time of the projected and unprojected definitions of the couplings, and of the squared topological charge, obtained with the standard and the PTBC algorithms for the 3 simulations points corresponding to a LCP with $l = 1.1$ fm. For the finest lattice spacing explored, only an upper bound on the auto-correlation time of $Q^2$ and of $\lambda_{\rm TGF}^{(\rm noproj)}$ could be set for the simulation with the standard algorithm, since no fluctuation of the topological charge was observed. In both cases, the auto-correlation time was expressed in units of lattice sweeps in order to make a fair comparison among the two algorithms. This means that the auto-correlation time was in both cases multiplied by the number of over-relaxation sweeps per heat-bath sweep, $n_{\rm ov}$, and, in the case of PTBC, also by the number of replicas $N_r$.

lattice spacing, and by more than two orders of magnitude for the finest one. Concerning the auto-correlation time of the unprojected coupling, we observe that the gain attained with PTBC is essentially of the same order of magnitude, while for projected couplings is much smaller, as it is about a factor of $\sim 2-3$. Being the PTBC algorithm tailored to improve the evolution of the topological charge, this is a further indication, in addition to our results for the coupling, that the fluctuations of the global topological charge seem rather decoupled from those of the coupling once projected onto a fixed topological sector.

### 4.2 Impact of topology projection on the step-scaling function

We now aim at probing the impact of topology on step scaling following the strategy earlier outlined in Sec. 2, which will be now spelled out in more detail.

- We fix a target value for $\lambda^{(0)}_{\rm TGF}(\mu = 2\mu_{\rm had}) = u_{\rm tg}$ on the LCP1. Since we have shown that the projected and the unprojected couplings give consistent results using both algorithms, we can choose any of the determinations of the previous section to fix $u_{\rm tg}$. We chose:

$$u_{\rm tg} = \lambda^{(0)}_{\rm TGF}(3b = 7, L = 24)\Big|_{\rm Standard} = 13.9063406. \tag{4.2}$$

  This point corresponds to take step 1 described in Sec. 2.

- We now consider the results for the renormalized coupling obtained for the same bare couplings of LCP1, but on doubled lattices, our goal being to compute the continuum step-scaling function at $\mu_{\rm had}$:

$$\sigma_{\rm tg} \equiv \sigma(u_{\rm tg}) = \lambda_{\rm TGF}\left(\mu = \mu_{\rm had}\right)\Big|_{\lambda_{\rm TGF}(\mu = 2\mu_{\rm had}) = u_{\rm tg}}. \tag{4.3}$$

  This is done following the same procedure put forward in Ref. [22], spelled out here for clarity. Since the tuning of the lattices is not perfect, there is a small mismatch in the lattice determined values of $u_{\rm tg}$. To correct for that, we slightly shift the values of the lattice step-scaling function taking into account the shifts in $u$ required to match $u_{\rm tg}$, this is done according to the formula:

$$\Sigma\left(u_{\rm tg}, L\right) = \Sigma\left(u, L\right) - \frac{\Sigma^2\left(u, L\right)}{u^2}\left(u - u_{\rm tg}\right), \tag{4.4}$$

  where $\Sigma(u, L)$ stands for the value of the coupling obtained for the simulation point $(b, L)$ and corresponding to the coupling $u$ obtained for the simulation point $(b, L/2)$. The relation used to determine $\Sigma\left(u_{\rm tg}, L\right)$ follows from the fact that, at leading order of perturbation theory, one expects $1/\Sigma(u) - 1/u =$ constant. Finally, the values of $\Sigma(u_{\rm tg}, L)$ are extrapolated to the continuum limit, defining:

$$\sigma_{\rm tg} = \lim_{1/L \to 0} \Sigma(u_{\rm tg}, L) \tag{4.5}$$

  This point corresponds to take step 2 described in Sec. 2. In Fig. 7 we report the continuum extrapolations of $\Sigma(u_{\rm tg}, L)$ obtained using the data shown in Sec. 4.1 for the $Q = 0$ projected couplings, and obtained from the two different algorithms. As it can be observed, we obtain perfectly consistent values between them:

$$\sigma^{(0)}_{\rm tg} = 34.43(24), \qquad \text{(Standard)}, \tag{4.6}$$

$$\sigma^{(0)}_{\rm tg} = 34.61(29), \qquad \text{(PTBC)}. \tag{4.7}$$

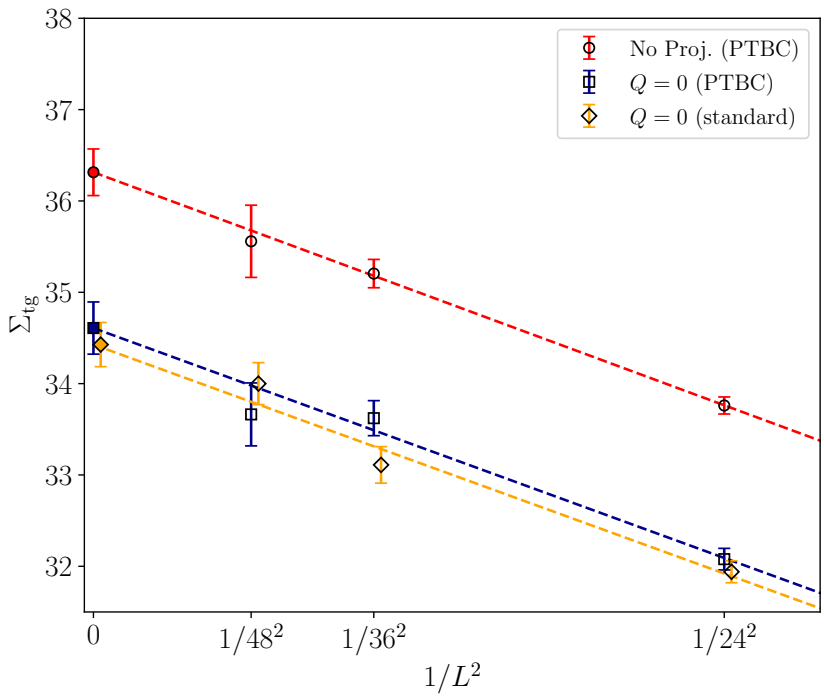


**Figure 7**. Continuum limit extrapolation of $\Sigma_{\rm tg} \equiv \Sigma(u_{\rm tg}, L)$ calculated using Eq. (4.5) from a projected and an unprojected definition of the coupling. In the former case, we show results obtained both using the PTBC and the standard algorithms.

Applying the same procedure to the unprojected coupling, which could only be reliably computed using the PTBC algorithm, one would obtain a continuum extrapolated step-scaling function:

$$\sigma_{\rm tg}^{\rm (noproj)} = 36.31(26), \qquad \text{(PTBC)}\,. \tag{4.8}$$

- As already discussed, topological fluctuations start to be important on this lattice volume, leading to different projected and unprojected couplings. It is therefore at this point where topology freezing and topology projection could have an effect on the determination of the step-scaling sequence. What we now want to check is precisely if, when $\lambda_{\rm TGF}^{(0)}$ is used to perform one step of the step-scaling sequence, a consistent change in the renormalization scale is obtained for the non-projected coupling too.

  With this purpose in mind, we determined the bare couplings $b$ that lead to a value of the renormalized coupling $\lambda_{\rm TGF}^{(0)} = \sigma_{\rm tg}^{(0)} = 34.43$, cf. Eq. (4.6).[5] This defines the line of constant physics dubbed as LCP2 in Tab. 1. If the projection of the coupling does not introduce a bias, and thus it is a legitimate and consistent way of defining an LCP, this should also be a proper LCP for the unprojected renormalized coupling, leading to a value that agrees with what we have earlier found for the continuum extrapolation of the unprojected step scaling function: $\sigma_{\rm tg}^{\rm (noproj)} = 36.31(26)$, cf. Eq. (4.8)

[5]The tuning of the bare couplings $b$ is done as indicated in Sec. 3.4 of Ref. [22].

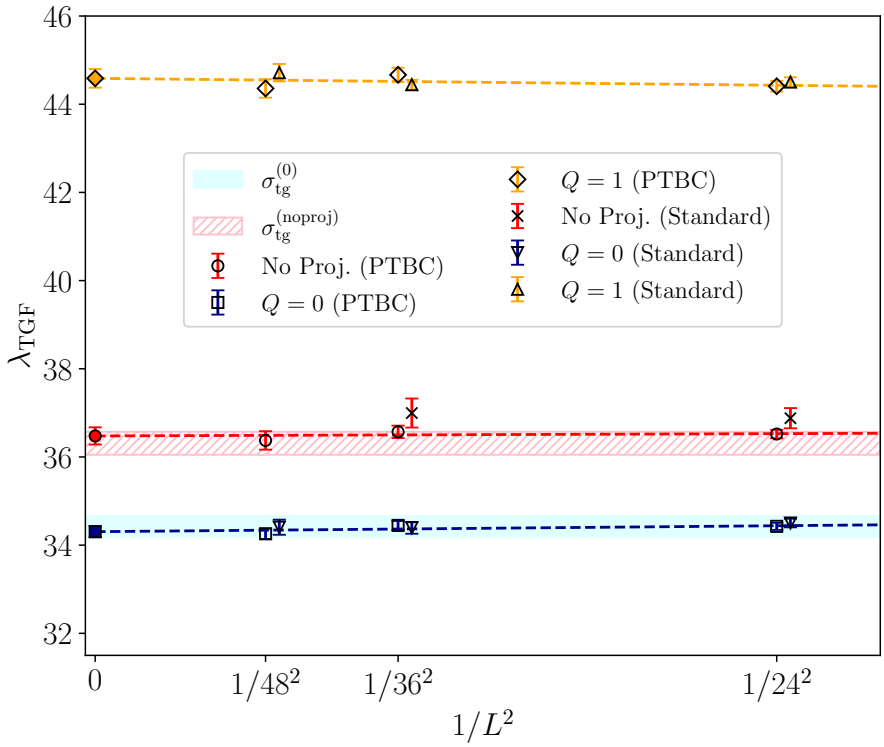


**Figure 8**. Extrapolation towards the continuum limit of the projected and unprojected couplings obtained with the PTBC algorithm for the 3 simulations points corresponding to a LCP with $l = 1.1$ fm, tuned to achieve a constant value of $\lambda_{\rm TGF}^{(0)} = \sigma_{\rm tg}^{(0)} = 34.42(24)$ (uniform shaded band), compared with the results obtained with the standard algorithm. The dashed shaded area represents $\sigma_{\rm tg}^{(\rm noproj)} = 36.31(26)$ obtained with the PTBC algorithm.

Finally, let us present the results of this test. The determination of the projected and unprojected couplings obtained on the LCP2 is shown in Fig. 8. The results obtained with parallel tempering for the unprojected coupling show no visible dependence on $L$ within the achieved per mil accuracy, and agree perfectly with the continuum-extrapolated target value $\sigma_{\rm tg}^{(\rm noproj)} = 36.31(26)$ earlier obtained in Eq. (4.8), represented by the dashed shaded area in the plot. Moreover, also in this case we find perfect agreement between the results obtained with the PTBC and the standard algorithms as far as the projected couplings are concerned. This piece of evidence completes the plan outlined at the beginning of this section, and fully confirms the reliability of topology projection for the purpose of calculating the step-scaling function, and hence the $\Lambda$-parameter.

As a by-product of our investigation, by virtue of the adoption of the parallel tempering algorithm, we were also able to reliably compute two topological observables, namely, the topological susceptibility,

$$t_0^2\chi = \left(\frac{\sqrt{t_0}}{a}\right)^4 \frac{\langle Q^2\rangle}{\tilde{L}^2 L^2}, \tag{4.9}$$

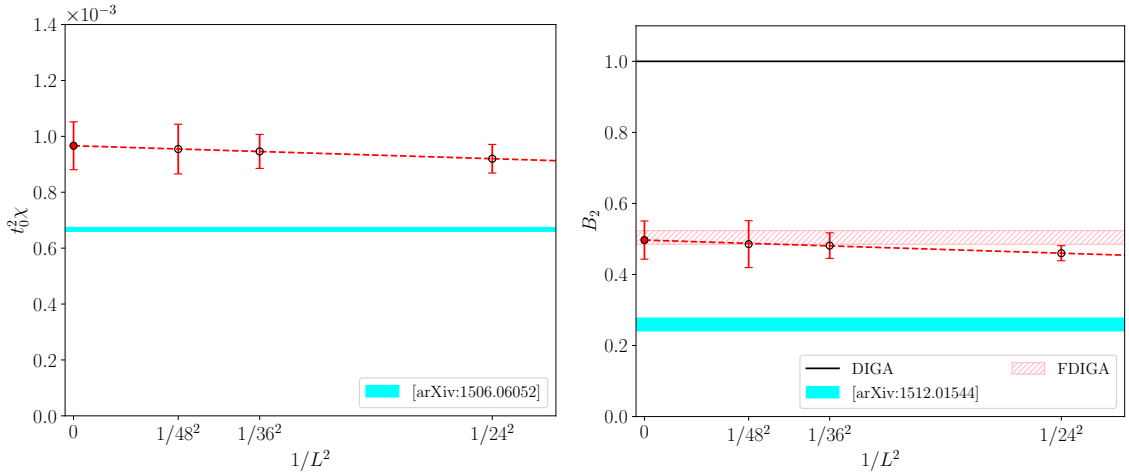


**Figure 9**. Continuum limit of the topological susceptibility $t_0^2\chi$ and of the quartic coefficient $B_2$ obtained with the PTBC algorithm for the 3 simulations points corresponding to a LCP with $l = 1.1$ fm. The infinite-volume estimates of $t_0^2\chi$ and of $B_2$, displayed as uniform shaded areas, are taken from Refs. [61, 73]. The dashed shaded area and the solid line represent instead the predictions for $B_2$ obtained using, respectively, the FDIGA and the DIGA.

and the dimensionless quartic coefficient $B_2$,[6]

$$B_2 = \frac{\langle Q^4 \rangle - 3\,\langle Q^2 \rangle^2}{\langle Q^2 \rangle}. \tag{4.10}$$

Remarkably, we observe that both quantities show extremely mild lattice artifacts when computed along the LCP2, as it can be seen from Fig. 9. This is yet a further confirmation that the calibration of the LCP done according to the $Q = 0$ projected coupling is a legitimate LCP also for topology-related quantities. This is actually not surprising, as, of course, $\langle Q^2 \rangle$ and $\lambda_{\rm TGF}^{\rm (noproj)}$ are not unrelated. In particular, recalling that we are working in a regime where $\langle Q^2 \rangle$ is small, the following approximate relation holds:

$$\begin{aligned} \lambda_{\rm TGF}^{\rm (noproj)} &\simeq \frac{P_0 \lambda_{\rm TGF}^{(0)} + 2P_1 \lambda_{\rm TGF}^{(1)}}{P_0 + 2P_1} \\ &\simeq \frac{1}{1 + \langle Q^2 \rangle} \lambda_{\rm TGF}^{(0)} + \langle Q^2 \rangle\, \lambda_{\rm TGF}^{(1)}, \qquad \langle Q^2 \rangle \simeq 2\frac{P_1}{P_0}. \end{aligned} \tag{4.11}$$

As a side note, we observe that our continuum determination of the topological susceptibility $t_0^2\chi = 9.66(88) \cdot 10^{-4}$ differs from the one obtained in Ref. [61] on a much larger volume, $t_0^2\chi = 6.67(7) \cdot 10^{-4}$, see Fig. 9 on the left. This is expected, and it is a finite-volume effect, which are known to be important for lattice sizes below $\sim 1.4$ fm. Finite-volume effects can be also seen in our continuum determination of $B_2 = 0.497(54)$, which also differs from the large-volume result of Ref. [73], $B_2 = 0.259(30)$, see Fig. 9 on the right. Remarkably, in this case we observe that our value is in perfect agreement with the one that can be obtained from the so-called Fractional Dilute Instanton Gas Approximation (FDIGA),

[6] Sometimes, the different definition $b_2 = -B_2/12$ is employed in the literature.

$B_2^{(\mathrm{FDIGA})} = 0.504(19)$ (see App. B for more details). The ordinary Dilute Instanton Gas Approximation (DIGA) [74, 75], instead, does not clearly work in this regime, as it would yield $B_2^{(\mathrm{DIGA})} = 1$. This result perfectly matches other theoretical and numerical evidence pointing out that, in the presence of TBCs, the semi-classical regime of SU($N$) Yang–Mills theories can be accurately described in terms of fractional instantons, see Ref. [82] for a recent review and for further references.

## 5 Conclusions

We have presented a new investigation of the role played by topology in the determination of the renormalized strong coupling from lattice simulations, with the goal of assessing the possible systematic effects introduced by topological freezing in the determination of the SU(3) pure-Yang–Mills $\Lambda$-parameter.

Our investigation combines twisted volume reduction and the gradient flow according to the setup of Ref. [22], with the SU($N$) Parallel Tempering on Boundary Conditions algorithm implementation of Ref. [33], suitably generalized to include TBCs, to accurately determine the step-scaling function, corresponding to the sequence $\mu_{\mathrm{had}} \to 2\mu_{\mathrm{had}}$, avoiding the effects of topological freezing. As a matter of fact, the PTBC algorithm allows to achieve a reduction of the auto-correlation time of the topological charge by up to two orders of magnitude compared to the standard algorithm.

Results obtained with parallel tempering show that topology projection works for the strong coupling even in the presence of severe topological freezing, as results obtained for the $Q = 0$ projected coupling with both algorithms always turn out to be in perfect agreement among themselves at the per mil accuracy we reached. Moreover, we showed that when results obtained with topology projection and the standard algorithm are employed to calibrate the parameters of an LCP with fixed projected renormalized coupling, this procedure also yields an LCP for the unprojected coupling, and for other topology-related quantities such as the topological susceptibility, computed using the PTBC algorithm. These findings imply that topology projection in the presence of topological freezing leads to the same step-scaling sequence that would have been otherwise obtained with the unprojected coupling, and thus ultimately to the same $\Lambda$-parameter.

Our current results can be expanded in several directions. For instance, it would be interesting to further investigate topology projection on small volumes by combining our twisted PTBC setup with the multicanonical algorithm, which can largely improve the sampling of rare volume-suppressed topological fluctuations. It would also be very interesting to extend our investigation to larger values of $N$ in order to study the large-$N$ limit of the $\Lambda$-parameter, which is an extremely interesting theoretical topic. To this end, it is crucial to check the effects of topology freezing on the scale setting procedure at large $N$, which can be efficiently achieved adopting the PTBC algorithm.

## Acknowledgements

It is a pleasure to thank Alberto Ramos for useful discussions and comments, and for carefully reading this manuscript. This work is partially supported by the Spanish Research Agency (Agencia Estatal de Investigación) through the grant IFT Centro de Excelencia Severo Ochoa CEX2020-001007-S and, partially, by grant PID2021-127526NB-I00, both funded by MCIN/AEI/10.13039/501100011033. This work has also been partially supported by the project "Non-perturbative aspects of fundamental interactions, in the Standard Model and beyond" funded by MUR, Progetti di Ricerca di Rilevante Interesse Nazionale (PRIN), Bando 2022, grant 2022TJFCYB (CUP I53D23001440006). We also acknowledge partial support from the project H2020-MSCAITN-2018-813942 (EuroPLEx) and the EU Horizon 2020 research and innovation programme, STRONG-2020 project, under grant agreement No. 824093. Numerical calculations have been performed partially on the `Marconi` machine at Cineca, based on the agreement between INFN and Cineca, under projects INF22_npqcd and INF23_npqcd, and partially on the `Finisterrae III` cluster at CESGA (Centro de Supercomputación de Galicia).

## Appendix

## A Raw data

In this appendix we report in Tabs. 3 and 4 all the numerical results shown in the plots in the main text. These two tables refer, respectively, to the PTBC and to the standard algorithms.

## B Dependence on $\theta$ with Fractional Dilute Instanton Gas Approximation

In this appendix we show how to derive the semiclassical expressions for the topological susceptibility and the quartic coefficient $B_2$ in the Fractional Dilute Instanton Gas Approximation (FDIGA). The main difference with the standard DIGA is the fact that the dilute gas is composed of instantons with fractional charge $Q = \pm 1/N = \pm 1/3$, as opposed to ordinary $Q = \pm 1$ instantons. These objects arise in a natural way on a torus with twisted boundary conditions and non-orthogonal twist ($n_{\mu\nu}\tilde{n}_{\mu\nu} \neq 0 \,(\mathrm{mod}\ N)$) [43] and have been the basis of the instanton liquid model of confinement put forward by González-Arroyo and collaborators; for a recent review and further references see [82]. Although our setup corresponds to an orthogonal twist, fractional instantons may still arise, provided that their total contribution to the topological charge amounts to an integer. In this context, Ref. [22] showed how the correlations observed in their small-to-intermediate volume TBC simulations between topological charge and coupling were quantitatively well described in this approximation. In this work, we have extended the analysis to the determination of the $B_2$ coefficient, showing that the prediction also works very well for this quantity in the appropriate regime.

The starting point for extracting the desired quantities is the dilute gas approximation for SU($N$) fractional instantons. As we have chosen an orthogonal twist, the total topo-

Parallel Tempering

| LCP1 ($l = 0.55$ fm) | | | |
|---|---|---|---|
| $L$ | $3 \times b$ | $\lambda_{\rm TGF}^{\rm (noproj)}$ | $\lambda_{\rm TGF}^{(0)}$ |
| 12 | 6.4881 | 13.9679(44) | 13.9503(47) |
| 18 | 6.7790 | 13.945(18) | 13.936(20) |
| 24 | 7.0000 | 13.945(25) | 13.953(29) |

| LCP1 with doubled $L$ | | | | |
|---|---|---|---|---|
| $L$ | $3 \times b$ | $\lambda_{\rm TGF}^{\rm (noproj)}$ | $\lambda_{\rm TGF}^{(0)}$ | $\lambda_{\rm TGF}^{(1)}$ |
| 24 | 6.459 | 34.128(90) | 32.31(12) | 42.78(18) |
| 36 | 6.765 | 35.46(11) | 33.80(15) | 43.10(23) |
| 48 | 6.992 | 35.81(36) | 33.94(30) | 43.35(18) |

| LCP2 ($l = 1.1$ fm) | | | | | | |
|---|---|---|---|---|---|---|
| $L$ | $3 \times b$ | $\lambda_{\rm TGF}^{\rm (noproj)}$ | $\lambda_{\rm TGF}^{(0)}$ | $\lambda_{\rm TGF}^{(1)}$ | $\langle Q^2 \rangle$ | $B_2$ |
| 24 | 6.459 | 36.520(96) | 34.426(81) | 44.41(12) | 0.1997(46) | 0.460(21) |
| 36 | 6.765 | 36.57(14) | 34.45(10) | 44.67(16) | 0.2050(78) | 0.481(36) |
| 48 | 6.992 | 36.37(21) | 34.26(12) | 44.36(21) | 0.207(16) | 0.485(66) |

**Table 3**. Summary of the obtained results using the PTBC algorithm.

logical charge remains quantized in integer units. This constraint must be applied when formulating the dilute gas fractional instanton partition function, which, when restricted to the sector of topological charge $Q$, reads as follows:

$$Z_Q = \mathcal{C} \sum_{n,\overline{n}} \frac{1}{n!\overline{n}!} (RV)^{n+\overline{n}} \delta(n - \overline{n} - NQ)\,, \tag{B.1}$$

where $R$ stands for the probability of creating a fractional instanton per unit volume $V$. From this expression, the $\theta$-dependent FDIGA partition function can be easily derived to be [22, 76, 83]:

$$Z(\theta) \equiv \sum_{Q \in \mathbf{Z}} e^{iQ\theta} Z_Q = \frac{\mathcal{C}}{N} \sum_{k=1}^{N} \exp\left\{ x \cos\left( \frac{\theta + 2\pi k}{N} \right) \right\}\,, \tag{B.2}$$

where $x = 2RV$; the reader is referred to Ref. [22] for more details on how to derive this expression. Taking derivatives of $Z(\theta)$ with respect to $\theta$, it is now trivial to derive the expressions for $\langle Q^2 \rangle$ and $\langle Q^4 \rangle$ in this approximation. For the SU(3) topological susceptibility, one obtains for instance:

$$V\chi(x) = \langle Q^2 \rangle (x) = \frac{x}{18} \left( 2 - \frac{3(2+x)}{2 + e^{3x/2}} \right)\,, \tag{B.3}$$

Standard

| LCP1 ($l = 0.55$ fm) | | | |
|---|---|---|---|
| $L$ | $3 \times b$ | $\lambda_{\rm TGF}^{\rm (noproj)}$ | $\lambda_{\rm TGF}^{(0)}$ |
| 12 | 6.4881 | 13.971(13) | 13.948(11) |
| 18 | 6.7790 | 13.939(13) | 13.938(11) |
| 24 | 7.0000 | 13.903(26) | 13.906(22) |

| LCP1 with doubled $L$ | | | | |
|---|---|---|---|---|
| $L$ | $3 \times b$ | $\lambda_{\rm TGF}^{\rm (noproj)}$ | $\lambda_{\rm TGF}^{(0)}$ | $\lambda_{\rm TGF}^{(1)}$ |
| 24 | 6.4881 | 33.94(21) | 32.17(11) | 42.96(23) |
| 36 | 6.7990 | 35.19(99) | 33.29(19) | 43.85(41) |
| 48 | 7.0000 | - | 34.00(20) | 43.94(90) |

| LCP2 ($l = 1.1$ fm) | | | | |
|---|---|---|---|---|
| $L$ | $3 \times b$ | $\lambda_{\rm TGF}^{\rm (noproj)}$ | $\lambda_{\rm TGF}^{(0)}$ | $\lambda_{\rm TGF}^{(1)}$ |
| 24 | 6.459 | 36.88(23) | 34.501(98) | 44.50(11) |
| 36 | 6.765 | 37.00(33) | 34.39(13) | 44.44(11) |
| 48 | 6.992 | - | 34.31(17) | 44.72(20) |

**Table 4**. Summary of the obtained results using the standard algorithm.

while the result for $B_2$ in SU(3) is given by:

$$B_2(x) = \frac{1}{9} + \frac{x(2+x)}{2(2+e^{3x/2})} - \frac{x^2(8+x)}{8-8e^{3x/2}+12x}. \tag{B.4}$$

To determine $B_2$ from Eq. (B.4), it is necessary to first determine the input quantity $x = 2RV$. Given the unreliability of the semi-classical approximation to this end, this can be done by inverting Eq. (B.3), using the value of the topological susceptibility measured on the lattice as input. More precisely, we found $\langle Q^2 \rangle = 0.209(12)$, leading to $x = 2.322(82)$ and to $B_2 = 0.504(19)$.

## References


[1] M. Dalla Brida, *Past, present, and future of precision determinations of the QCD parameters from lattice QCD*, *Eur. Phys. J. A* **57** (2021) 66 [2012.01232].

[2] K. Maltman, D. Leinweber, P. Moran and A. Sternbeck, *The Realistic Lattice Determination of $\alpha(s)(M(Z))$ Revisited*, *Phys. Rev. D* **78** (2008) 114504 [0807.2020].

[3] PACS-CS collaboration, S. Aoki et al., *Precise determination of the strong coupling constant in $N_f$ = 2+1 lattice QCD with the Schrodinger functional scheme*, *JHEP* **10** (2009) 053 [0906.3906].

[4] C. McNeile, C. T. H. Davies, E. Follana, K. Hornbostel and G. P. Lepage, *High-Precision c and b Masses, and QCD Coupling from Current-Current Correlators in Lattice and Continuum QCD*, *Phys. Rev. D* **82** (2010) 034512 [1004.4285].

[5] B. Chakraborty, C. T. H. Davies, B. Galloway, P. Knecht, J. Koponen, G. C. Donald et al., *High-precision quark masses and QCD coupling from $n_f = 4$ lattice QCD*, *Phys. Rev. D* **91** (2015) 054508 [1408.4169].

[6] ALPHA collaboration, M. Bruno, M. Dalla Brida, P. Fritzsch, T. Korzec, A. Ramos, S. Schaefer et al., *QCD Coupling from a Nonperturbative Determination of the Three-Flavor $\Lambda$ Parameter*, *Phys. Rev. Lett.* **119** (2017) 102001 [1706.03821].

[7] S. Cali, K. Cichy, P. Korcyl and J. Simeth, *Running coupling constant from position-space current-current correlation functions in three-flavor lattice QCD*, *Phys. Rev. Lett.* **125** (2020) 242002 [2003.05781].

[8] TUMQCD collaboration, A. Bazavov, N. Brambilla, X. Garcia i Tormo, P. Petreczky, J. Soto, A. Vairo et al., *Determination of the QCD coupling from the static energy and the free energy*, *Phys. Rev. D* **100** (2019) 114511 [1907.11747].

[9] C. Ayala, X. Lobregat and A. Pineda, *Determination of $\alpha(M_z)$ from an hyperasymptotic approximation to the energy of a static quark-antiquark pair*, *JHEP* **09** (2020) 016 [2005.12301].

[10] Flavour Lattice Averaging Group (FLAG) collaboration, Y. Aoki et al., *FLAG Review 2021*, *Eur. Phys. J. C* **82** (2022) 869 [2111.09849].

[11] Particle Data Group collaboration, R. L. Workman and Others, *Review of Particle Physics*, *PTEP* **2022** (2022) 083C01.

[12] ALPHA collaboration, M. Dalla Brida, R. Höllwieser, F. Knechtli, T. Korzec, A. Ramos and R. Sommer, *Non-perturbative renormalization by decoupling*, *Phys. Lett. B* **807** (2020) 135571 [1912.06001].

[13] L. Del Debbio and A. Ramos, *Lattice determinations of the strong coupling*, 2101.04762.

[14] N. Brambilla, X. Garcia i Tormo, J. Soto and A. Vairo, *Precision determination of $r_0\Lambda_{\overline{\rm MS}}$ from the QCD static energy*, *Phys. Rev. Lett.* **105** (2010) 212001 [1006.2066].

[15] M. Asakawa, T. Hatsuda, T. Iritani, E. Itou, M. Kitazawa and H. Suzuki, *Determination of Reference Scales for Wilson Gauge Action from Yang–Mills Gradient Flow*, 1503.06516.

[16] M. Kitazawa, T. Iritani, M. Asakawa, T. Hatsuda and H. Suzuki, *Equation of State for SU(3) Gauge Theory via the Energy-Momentum Tensor under Gradient Flow*, *Phys. Rev. D* **94** (2016) 114512 [1610.07810].

[17] K.-I. Ishikawa, I. Kanamori, Y. Murakami, A. Nakamura, M. Okawa and R. Ueno, *Non-perturbative determination of the $\Lambda$-parameter in the pure SU(3) gauge theory from the twisted gradient flow coupling*, *JHEP* **12** (2017) 067 [1702.06289].

[18] N. Husung, M. Koren, P. Krah and R. Sommer, *SU(3) Yang Mills theory at small distances and fine lattices*, *EPJ Web Conf.* **175** (2018) 14024 [1711.01860].

[19] M. Dalla Brida and A. Ramos, *The gradient flow coupling at high-energy and the scale of SU(3) Yang–Mills theory*, *Eur. Phys. J. C* **79** (2019) 720 [1905.05147].

[20] A. Nada and A. Ramos, *An analysis of systematic effects in finite size scaling studies using the gradient flow*, *Eur. Phys. J. C* **81** (2021) 1 [2007.12862].

[21] N. Husung, A. Nada and R. Sommer, *Yang Mills short distance potential and perturbation theory*, *PoS* **LATTICE2019** (2020) 263.

[22] E. I. Bribian, J. L. D. Golan, M. Garcia Perez and A. Ramos, *Memory efficient finite volume schemes with twisted boundary conditions*, *Eur. Phys. J. C* **81** (2021) 951 [2107.03747].

[23] A. Hasenfratz, C. T. Peterson, J. van Sickle and O. Witzel, $\Lambda$ *parameter of the SU(3) Yang-Mills theory from the continuous $\beta$ function*, *Phys. Rev. D* **108** (2023) 014502 [2303.00704].

[24] R. Narayanan and H. Neuberger, *Infinite N phase transitions in continuum Wilson loop operators*, *JHEP* **03** (2006) 064 [hep-th/0601210].

[25] R. Lohmayer and H. Neuberger, *Continuous smearing of Wilson Loops*, *PoS* **LATTICE2011** (2011) 249 [1110.3522].

[26] M. Luscher, *Trivializing maps, the Wilson flow and the HMC algorithm*, *Commun. Math. Phys.* **293** (2010) 899 [0907.5491].

[27] P. Fritzsch, A. Ramos and F. Stollenwerk, *Critical slowing down and the gradient flow coupling in the Schrödinger functional*, *PoS* **Lattice2013** (2014) 461 [1311.7304].

[28] B. Alles, G. Boyd, M. D'Elia, A. Di Giacomo and E. Vicari, *Hybrid Monte Carlo and topological modes of full QCD*, *Phys. Lett. B* **389** (1996) 107 [hep-lat/9607049].

[29] L. Del Debbio, G. M. Manca and E. Vicari, *Critical slowing down of topological modes*, *Phys. Lett. B* **594** (2004) 315 [hep-lat/0403001].

[30] ALPHA collaboration, S. Schaefer, R. Sommer and F. Virotta, *Critical slowing down and error analysis in lattice QCD simulations*, *Nucl. Phys. B* **845** (2011) 93 [1009.5228].

[31] D. Albandea, P. Hernández, A. Ramos and F. Romero-López, *Topological sampling through windings*, *Eur. Phys. J. C* **81** (2021) 873 [2106.14234].

[32] M. Hasenbusch, *Fighting topological freezing in the two-dimensional $CP^{N-1}$ model*, *Phys. Rev. D* **96** (2017) 054504 [1706.04443].

[33] C. Bonanno, C. Bonati and M. D'Elia, *Large-N $SU(N)$ Yang-Mills theories with milder topological freezing*, *JHEP* **03** (2021) 111 [2012.14000].

[34] M. Berni, C. Bonanno and M. D'Elia, *Large-N expansion and $\theta$-dependence of 2d $CP^{N-1}$ models beyond the leading order*, *Phys. Rev. D* **100** (2019) 114509 [1911.03384].

[35] C. Bonanno, M. D'Elia, B. Lucini and D. Vadacchino, *Towards glueball masses of large-N SU(N) pure-gauge theories without topological freezing*, *Phys. Lett. B* **833** (2022) 137281 [2205.06190].

[36] C. Bonanno, *Lattice determination of the topological susceptibility slope $\chi'$ of 2d $CP^{N-1}$ models at large $N$*, *Phys. Rev. D* **107** (2023) 014514 [2212.02330].

[37] C. Bonanno, M. D'Elia and L. Verzichelli, *The $\theta$-dependence of the SU(N) critical temperature at large N*, *JHEP* **02** (2024) 156 [2312.12202].

[38] C. Bonanno, C. Bonati, M. Papace and D. Vadacchino, *The $\theta$-dependence of the Yang-Mills spectrum from analytic continuation*, 2402.03096.

[39] M. Lüscher and S. Schaefer, *Lattice QCD without topology barriers*, *JHEP* **07** (2011) 036 [1105.4749].

[40] M. Lüscher and S. Schaefer, *Lattice QCD with open boundary conditions and twisted-mass reweighting*, *Comput. Phys. Commun.* **184** (2013) 519 [1206.2809].

[41] J. L. Dasilva Golán, C. Bonanno, M. D'Elia, M. García Pérez and A. Giorgieri, *The twisted gradient flow strong coupling with parallel tempering on boundary conditions*, *PoS* **LATTICE2023** (2024) 354 [2312.09212].

[42] M. Luscher, P. Weisz and U. Wolff, *A Numerical method to compute the running coupling in asymptotically free theories*, *Nucl. Phys. B* **359** (1991) 221.

[43] G. 't Hooft, *A Property of Electric and Magnetic Flux in Nonabelian Gauge Theories*, *Nucl. Phys. B* **153** (1979) 141.

[44] G. 't Hooft, *Confinement and Topology in Nonabelian Gauge Theories*, *Acta Phys. Austriaca Suppl.* **22** (1980) 531.

[45] A. Gonzalez-Arroyo and M. Okawa, *The Twisted Eguchi-Kawai Model: A Reduced Model for Large N Lattice Gauge Theory*, *Phys. Rev. D* **27** (1983) 2397.

[46] A. Gonzalez-Arroyo and M. Okawa, *A Twisted Model for Large N Lattice Gauge Theory*, *Phys. Lett. B* **120** (1983) 174.

[47] A. Gonzalez-Arroyo and M. Okawa, *Large N reduction with the Twisted Eguchi-Kawai model*, *JHEP* **07** (2010) 043 [1005.1981].

[48] M. Garcia Perez, A. Gonzalez-Arroyo and M. Okawa, *Volume independence for Yang–Mills fields on the twisted torus*, *Int. J. Mod. Phys. A* **29** (2014) 1445001 [1406.5655].

[49] M. García Pérez, *Prospects for large N gauge theories on the lattice*, *PoS* **LATTICE2019** (2020) 276 [2001.10859].

[50] T. Eguchi and H. Kawai, *Reduction of dynamical degrees of freedom in the large-N gauge theory*, *Phys. Rev. Lett.* **48** (1982) 1063.

[51] M. Lüscher, *Some Analytic Results Concerning the Mass Spectrum of Yang-Mills Gauge Theories on a Torus*, *Nucl. Phys. B* **219** (1983) 233.

[52] M. Lüscher, R. Narayanan, P. Weisz and U. Wolff, *The Schrödinger functional: A Renormalizable probe for nonAbelian gauge theories*, *Nucl. Phys. B* **384** (1992) 168 [hep-lat/9207009].

[53] A. Ramos, *The gradient flow running coupling with twisted boundary conditions*, *JHEP* **11** (2014) 101 [1409.1445].

[54] E. I. Bribian and M. Garcia Perez, *The twisted gradient flow coupling at one loop*, *JHEP* **03** (2019) 200 [1903.08029].

[55] M. Creutz, *Monte Carlo Study of Quantized $SU(2)$ Gauge Theory*, *Phys. Rev. D* **21** (1980) 2308.

[56] A. D. Kennedy and B. J. Pendleton, *Improved Heat Bath Method for Monte Carlo Calculations in Lattice Gauge Theories*, *Phys. Lett. B* **156** (1985) 393.

[57] M. Creutz, *Overrelaxation and Monte Carlo Simulation*, *Phys. Rev. D* **36** (1987) 515.

[58] M. Lüscher, *Properties and uses of the Wilson flow in lattice QCD*, *JHEP* **08** (2010) 071 [1006.4518].

[59] ALPHA collaboration, F. Knechtli, T. Korzec, B. Leder and G. Moir, *Power corrections from decoupling of the charm quark*, *Phys. Lett. B* **774** (2017) 649 [1706.04982].

[60] L. Giusti and M. Lüscher, *Topological susceptibility at $T > T_c$ from master-field simulations of the SU(3) gauge theory*, Eur. Phys. J. C **79** (2019) 207 [1812.02062].

[61] M. Cè, C. Consonni, G. P. Engel and L. Giusti, *Non-Gaussianities in the topological charge distribution of the SU(3) Yang–Mills theory*, Phys. Rev. D **92** (2015) 074502 [1506.06052].

[62] D. J. Gross, R. D. Pisarski and L. G. Yaffe, *Qcd and instantons at finite temperature*, Rev. Mod. Phys. **53** (1981) 43.

[63] S. Borsányi, M. Dierigl, Z. Fodor, S. D. Katz, S. W. Mages, D. Nógrádi et al., *Axion cosmology, lattice QCD and the dilute instanton gas*, Phys. Lett. B **752** (2016) 175 [1508.06917].

[64] P. Petreczky, H.-P. Schadler and S. Sharma, *The topological susceptibility in finite temperature QCD and axion cosmology*, Phys. Lett. B **762** (2016) 498 [1606.03145].

[65] S. Borsányi, Z. Fodor, J. Guenther, K.-H. Kampert, S. D. Katz, T. Kawanai et al., *Calculation of the axion mass based on high-temperature lattice quantum chromodynamics*, Nature **539** (2016) 69 [1606.07494].

[66] P. T. Jahn, G. D. Moore and D. Robaina, *$\chi_{top}(T \gg T_c)$ in pure-glue QCD through reweighting*, Phys. Rev. D **98** (2018) 054512 [1806.01162].

[67] C. Bonati, M. D'Elia, G. Martinelli, F. Negro, F. Sanfilippo and A. Todaro, *Topology in full QCD at high temperature: a multicanonical approach*, JHEP **11** (2018) 170 [1807.07954].

[68] M. P. Lombardo and A. Trunin, *Topology and axions in QCD*, Int. J. Mod. Phys. A **35** (2020) 2030010 [2005.06547].

[69] S. Borsányi and D. Sexty, *Topological susceptibility of pure gauge theory using Density of States*, Phys. Lett. B **815** (2021) 136148 [2101.03383].

[70] A. Athenodorou, C. Bonanno, C. Bonati, G. Clemente, F. D'Angelo, M. D'Elia et al., *Topological susceptibility of $N_f = 2 + 1$ QCD from staggered fermions spectral projectors at high temperatures*, JHEP **10** (2022) 197 [2208.08921].

[71] C. Bonanno, M. D'Elia and F. Margari, *Topological susceptibility of the 2D $CP^1$ or O(3) nonlinear $\sigma$ model: Is it divergent or not?*, Phys. Rev. D **107** (2023) 014515 [2208.00185].

[72] B. Lucini, D. Mason, M. Piai, E. Rinaldi and D. Vadacchino, *First-order phase transitions in Yang-Mills theories and the density of state method*, Phys. Rev. D **108** (2023) 074517 [2305.07463].

[73] C. Bonati, M. D'Elia and A. Scapellato, *$\theta$ dependence in $SU(3)$ Yang-Mills theory from analytic continuation*, Phys. Rev. D **93** (2016) 025028 [1512.01544].

[74] D. J. Gross, R. D. Pisarski and L. G. Yaffe, *QCD and Instantons at Finite Temperature*, Rev. Mod. Phys. **53** (1981) 43.

[75] T. Schäfer and E. V. Shuryak, *Instantons in QCD*, Rev. Mod. Phys. **70** (1998) 323 [hep-ph/9610451].

[76] P. van Baal, *Twisted Boundary Conditions: A Nonperturbative Probe for Pure Nonabelian Gauge Theories*, Ph.D. Thesis, Utrecht U., 7, 1984.

[77] RTN collaboration, M. Garcia Perez et al., *Instanton like contributions to the dynamics of Yang-Mills fields on the twisted torus*, Phys. Lett. B **305** (1993) 366 [hep-lat/9302007].

[78] M. Garcia Perez, A. Gonzalez-Arroyo and P. Martinez, *From perturbation theory to confinement: How the string tension is built up*, *Nucl. Phys. B Proc. Suppl.* **34** (1994) 228 [hep-lat/9312066].

[79] A. Gonzalez-Arroyo, P. Martinez and A. Montero, *Gauge invariant structures and confinement*, *Phys. Lett. B* **359** (1995) 159 [hep-lat/9507006].

[80] A. Gonzalez-Arroyo and P. Martinez, *Investigating Yang-Mills theory and confinement as a function of the spatial volume*, *Nucl. Phys. B* **459** (1996) 337 [hep-lat/9507001].

[81] V. P. Nair and R. D. Pisarski, *Fractional topological charge in SU(N) gauge theories without dynamical quarks*, *Phys. Rev. D* **108** (2023) 074007 [2206.11284].

[82] A. Gonzalez-Arroyo, *On the fractional instanton liquid picture of the Yang-Mills vacuum and Confinement*, 2302.12356.

[83] P. van Baal, *QCD in a finite volume*, hep-ph/0008206.